Electronic structure of graphene tubules based on C_{60}

Riichiro Saito,* Mitsutaka Fujita,† G. Dresselhaus, and M. S. Dresselhaus
Department of Physics, Massachusetts Institute of Technology, Cambridge, Massachusetts 02139
(Received 2 December 1991)

The electronic structures of some possible carbon fibers nucleated from the hemisphere of a C_{60} molecule are presented. A one-dimensional electronic band-structure model of such carbon fibers, having not only rotational symmetry but also screw axes, is derived by folding the two-dimensional energy bands of graphite. A simple tight-binding model shows that some fibers are metallic and are stable against perturbations of the one-dimensional energy bands and the mixing of σ and π bands due to the curvature of the circumference of the fiber.

I. INTRODUCTION

Recent models of carbon fibers have focused attention on highly ordered fiber structures based on fullerenes.[1–4] Carbon fibers are a low-dimensional carbon system that has been widely used in applications as a conductive, lightweight, and strong material.[5] Because of several possible hybridizations of the carbon $2s$ and $2p$ orbitals, materials of different dimensionalities can be formed such as diamond [three dimensional (3D)], graphite (2D), graphene tubules (1D)[1] and fullerenes (0D)[6–9]. For graphite, carbon fibers, and fullerenes, the sp^2 hybridization of hexagonal (or pentagonal) carbon networks is essential to model their electronic structures.

Graphite is a semimetal due to the weak coupling between two graphite layers. Graphite is further known to have a zero energy gap as the interlayer interaction goes to zero.[10] In the case of a C_{60}, the Kekulé structure appears because of the lower symmetry of the pentagon[11] which results in semiconducting behavior with an energy gap of 1.9 eV.[12] Carbon fibers with a nanometer radius, which are considered in this paper, have one-dimensional energy bands. One-dimensional energy bands are generally unstable under certain symmetry-lowering distortions even if the fiber has a finite density of states at the Fermi energy.[13] However, when we increase the radius of the fiber, the electronic structure of the fiber becomes close to that of graphite which is known to be stable under such distortions, since a graphene (i.e., a single layer of 3D graphite) sheet is a zero-energy-gap semiconductor. Thus some changes in the phase diagram would be expected upon increasing the fiber diameter. Furthermore, for a very small diameter fiber the curvature of the fiber causes a hybridization of sp^3 orbitals which sensitively affects the electronic structure and depends on the geometry of the fiber and on the fiber diameter. In addition to the effects of fiber diameter, the chirality of the fiber represents a possible structural modification which in turn modifies the electronic structure.

In this paper first we discuss the electronic structure of two typical examples of nonchiral carbon fibers. Then we show that the electronic structure for the π band of a carbon fiber is metallic within a simple tight-binding approximation, and that the electronic structure of a chiral fiber can also be explained within this scheme. Further, in order to examine the mixing effect of the hybridization of the sp^3 orbitals due to the fiber curvature, we diagonalize the tight-binding Hamiltonian in which we consider both σ and π bands. Finally, we discuss the instability of carbon fibers for some possible perturbations as a function of the fiber radius.

In this work a carbon fiber is considered to be a roll of graphene layers. Transmission electron-microscope observations show that in a nanometer carbon tubule, several (two or more) graphene planes are rolled into independent cylinders within a diameter of 2–6 nm.[2] Though a few graphite layers are stacked layer by layer in a fiber, we can neglect the weak interlayer interaction between adjacent layers in a fiber since the layer stacking is not commensurate.

Once the innermost tube is formed, it might be easy to stack other graphene cylindrical layers, based on our knowledge of the thickening process for a vapor-grown carbon fiber.[5] Thus the formation of the innermost tube of a fiber is a key to the growth of a carbon fiber, which should be nucleated at one end, from a small diameter carbon cluster in the vapor phase. At this end some pentagons are necessary to nucleate a ball-like structure with a large curvature. It is reasonable to consider that the hemisphere of C_{60} can be one nucleating end of such a fiber. Basically there are two simple possibilities (among others) for nucleating a fiber, as shown in Fig. 1. In this figure we show the molecular structure of (a) C_{60}, and of (b) armchair and (c) zigzag dissection cuts of C_{60} (Ref. 1) in which their boundary atoms are arranged in a *cis* or *trans* form of a carbon chain by analogy to the case of polyacetylene.[14] In a physical nucleation cluster for a graphene tubule[1], some defect could be present, which would make the cylindrical (fiber) growth mode lower in energy than the spherical (fullerene) growth mode.

There are 10 and 9 carbon atoms at the surface of the caps in Figs. 1(a) and 1(b), respectively and, correspondingly, a pentagon and a hexagon at the center

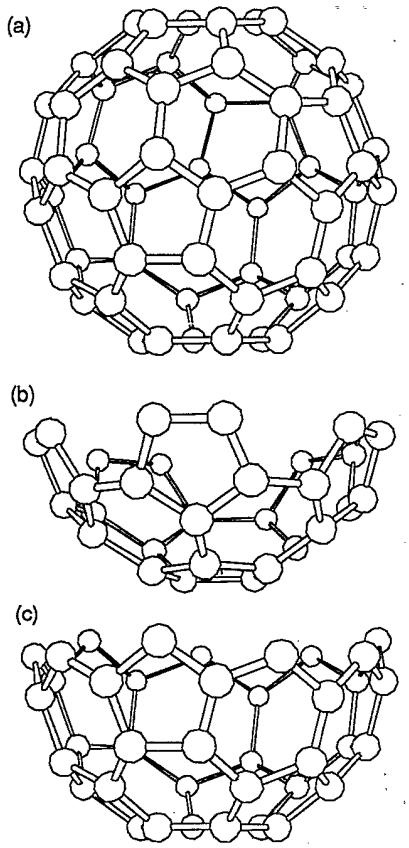

FIG. 1. (a) C_{60}, (b) armchair cut, and (c) zigzag cut of C_{60} to form caps for armchair and zigzag fibers.

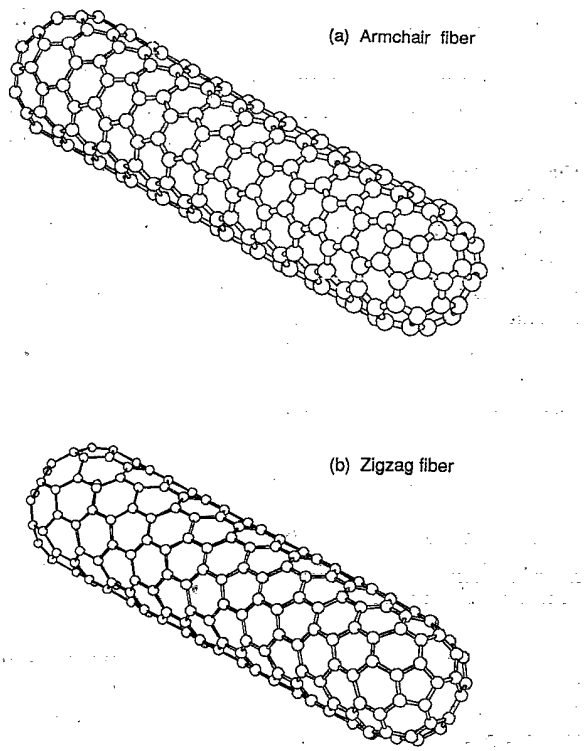

FIG. 2. Atomic arrangements of carbon atoms in the (a) armchair fiber and (b) zigzag fiber.

of the armchair and zigzag cuts. From Fig. 1 the two cuts have fivefold and threefold rotational symmetry for the armchair and zigzag fibers, respectively. From these cuts we can connect up the carbon fiber which consists of a cylinder of only hexagons in the two ways shown in Fig. 2. The fibers growing from the armchair and zigzag cuts will be called hereafter armchair and zigzag fibers, respectively.

There are many other possible fiber geometries based on a hexagonal network. Of particular interest are chiral fibers with a screw axis.[1] As discussed in Ref. 1, a single vector is sufficient for specifying fibers with a screw axis. In Fig. 3(a), we show an example of the vector, $\overrightarrow{AA'}$ in the 2D graphene layer in which we connect two parallel, dotted lines that are perpendicular to the vector, and specify the fiber. When we roll the graphene sheet, the line segment of the vector $\overrightarrow{AA'}$ becomes the circumference of the fiber and thus the dotted lines are in the direction parallel to the fiber axis. In Fig. 3(b) we show the atomic arrangement and the spiral structure of the corresponding fiber. It is important to note here that we can make such a chiral fiber, without any special distortion of the fiber bonding angles arising from the screw axis, other than the introduction of curvature to the hexagons through the rolling process.

Referring to Fig. 3(a), if we change the tilt angle from

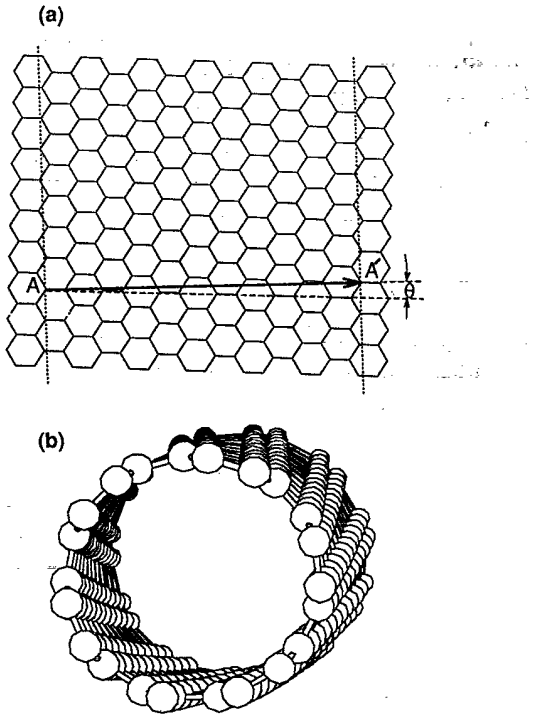

FIG. 3. (a) The vector $\overrightarrow{AA'}$ specifies a chiral fiber. We connect two dotted lines, normal to $\overrightarrow{AA'}$ at A and A', to form a chiral fiber. (b) Atomic arrangement of the corresponding chiral fiber. The vector specifying an armchair has $\theta = 0°$ and a zigzag fiber has $\theta = 30°$.

0° to 30°, we can go from an armchair to a zigzag fiber, so that the use of a single vector to uniquely specify the fiber geometry relates the armchair and zigzag fibers as limiting cases of a sequence of possible chiral fibers. This approach thus provides a generalized framework for describing a whole family of carbon fibers (graphene tubules), one layer in thickness.

In Sec. II we first present the electronic structure of the two typical carbon fibers followed by that for the chiral fibers. Then we discuss the σ-π band-mixing effect due to the curvature of the fibers. In Sec. III the possible instability of the carbon fibers associated with a Peierls distortion is discussed. Finally in Sec. IV some general discussion and conclusions are given.

II. ELECTRONIC STRUCTURE

Let us now consider the electronic structure of these fibers. If the fiber is sufficiently long, we can neglect the effect of the ends. When we cut and unroll a graphite cylinder parallel to the cylinder axis, we get a two-dimensional graphene plane in which translational symmetry exists in the direction of the fiber and periodic boundary conditions will be applied in the direction perpendicular to the axis. Thus we start by considering the electronic structure of the unrolled graphene plane with periodic boundary conditions in the transverse direction. In the case of graphite, the valence orbital is a $\pi(2p_z)$ orbital and there is no interaction between the π and $\sigma(2s$ and $2p_{x,y})$ orbitals because of their different symmetries. The mixing of π and σ orbitals due to the curvature of the fiber can be neglected as shown later, and thus we first consider only π bands.

Since the carbon atoms in a graphene plane can be divided into two sublattices A and B (bipartite lattice), the π bands of 2D graphite are derived from the following 2×2 Hamiltonian matrix $\mathcal{H}$:[10]

$$\mathcal{H} = \begin{pmatrix} 0 & h_0^* \\ h_0 & 0 \end{pmatrix}. \tag{1}$$

Here h_0 is the nearest-neighbor interaction between the A and B sublattices expressed as

$$h_0 = \gamma_0 \left\{ e^{ik_x a/\sqrt{3}} + 2e^{-ik_x a/2\sqrt{3}} \cos\left(\frac{k_y a}{2}\right) \right\}, \tag{2}$$

where $a = 1.42 \times \sqrt{3}$ Å is the lattice constant and γ_0 is nearest-neighbor transfer integral.[15] Diagonalizing the Hamiltonian of Eq. (1), we obtain the two-dimensional energy dispersion relation of graphite, $E_{2D}(k_x, k_y)$ as follows:

$$E_{2D}(k_x, k_y) = \pm\gamma_0 \left\{ 1 + 4\cos\left(\frac{\sqrt{3}k_x a}{2}\right)\cos\left(\frac{k_y a}{2}\right) + 4\cos^2\left(\frac{k_y a}{2}\right) \right\}^{1/2}. \tag{3}$$

For the two typical carbon fibers shown in Fig. 2, we just fold the Brillouin zone of graphite and introduce discrete values of the wave vector in the direction perpendicular to the fiber axis. As a result, a set of 1D energy dispersion relations is obtained by slicing up the 2D energy band structure of graphite in the circumferential direction. In Fig. 4 we show the real space unit cells and Brillouin zones for (a) the armchair fiber and (b) the zigzag fiber, respectively, where a_i and a_i' and b_i and b_i' $(i = 1, 2)$ are unit vectors and reciprocal vectors of the original 2D graphite and the fiber, respectively.

Writing the following relation for the periodic boundary condition associated with the armchair fiber,

$$k_x^m = \frac{m}{N_x}\frac{2\pi}{\sqrt{3}a} \quad (m = 1, \ldots, N_x) \text{ with } N_x = 5, \tag{4}$$

we get the 1D energy dispersion relations $E_m^a(k)$ for the armchair fiber:

$$E_m^a(k) = \pm\gamma_0 \left\{ 1 \pm 4\cos\left(\frac{m\pi}{5}\right)\cos\left(\frac{ka}{2}\right) + 4\cos^2\left(\frac{ka}{2}\right) \right\}^{1/2}$$

$$(-\pi < ka < \pi) \quad (m = 1, \ldots, 5), \tag{5}$$

in which k is a one-dimensional vector along the fiber axis and the plus and minus sign appearing under the square-root sign correspond to the unfolded and folded energy bands, respectively.

The energy bands for the zigzag fiber $E_m^z(k)$ can be obtained in a similar way by putting

$$k_y^m = \frac{m}{N_y}\frac{2\pi}{a} \quad (m = 1, \ldots, N_y) \quad \text{with} \quad N_y = 9, \tag{6}$$

as follows:

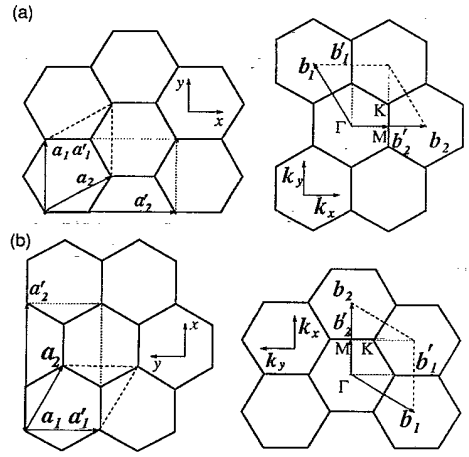

FIG. 4. Unit cell and Brillouin zone for (a) armchair and (b) zigzag fibers (dotted lines). Those for 2D graphite (dashed lines) are shown for comparison.

$$E_m^z(k) = \pm\gamma_0 \left\{ 1 \pm 4\cos\left(\frac{\sqrt{3}ka}{2}\right)\cos\left(\frac{m\pi}{9}\right) + 4\cos^2\left(\frac{m\pi}{9}\right)\right\}^{1/2}$$

$$\left(-\frac{\pi}{\sqrt{3}} < ka < \frac{\pi}{\sqrt{3}}\right) \quad (m = 1, \ldots, 9). \quad (7)$$

In Fig. 5 we show the normalized energy dispersion relations plotted as E/γ_0 vs k for (a) armchair and (b) zigzag fibers, respectively. For the rotational symmetry of group $D_{(2n+1)d}$ around the armchair ($n = 2$) and zigzag ($n = 4$) fibers, the energy bands can be degenerate up to a twofold degeneracy as shown in Table I. In Fig. 5 the eigenfunctions at $k = 0$ are labeled by the irreducible representations of $D_{(2n+1)d}$, in which the + and − superscripts denote the unfolded and folded energy bands, respectively. The thick lines in the figure denote the twofold energy bands with E_{1g}, E_{1u}, E_{2g}, E_{2u}, ..., symmetry and thus the number of bands appearing in the figure is smaller than $4m$ which is expected from Eqs. (5) and (7).

In the case of the armchair fiber, the energy bands are all (accidentally) degenerate at the zone boundary, since the boundary corresponds to the equienergy line of 2D graphite. To make a rectangular unit cell, we consider four carbon atoms per unit cell for both types of fibers, as shown in Fig. 4. The four carbon atoms in the unit cell are symmetrically equivalent, which causes the degeneracy of the energy bands. If we view these one-dimensional energy bands in the extended zone scheme, the dispersion relations are obtained by "slicing" the 2D energy dispersion relations of graphite along the directions of $k_x^{(m)} = \frac{m}{N_x}\frac{2\pi}{\sqrt{3}a}$ and $k_y^{(m)} = \frac{m}{N_y}\frac{2\pi}{a}$ for the armchair and the zigzag fibers, respectively. In terms of the number of distinct atoms per unit cell, we do not need such a large unit cell for fibers as is given in Fig. 4. The particular unit cells chosen are selected to simplify the specifications of the periodic boundary conditions for the fibers.

In both cases, we have two energy bands which cross

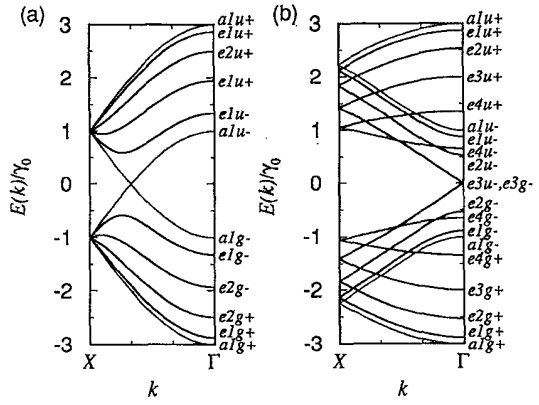

FIG. 5. 1D energy dispersion relations for (a) armchair and (b) zigzag fibers, labeled by the irreducible representations of group $D_{(2n+1)d}$ at $k = 0$. The A bands are nondegenerate and the E bands are doubly degenerate at a general k point.

the Fermi energy at $E = 0$ since the corresponding 2D graphite energy bands cross at the K point (corners of the hexagons) of the 2D Brillouin zone where the 2D energy bands are degenerate. Although the density of states is zero at the K point in the 2D case, we have a finite density of states at the K point in the present cases since these energy bands are one dimensional. Therefore, if there is no instability for a one-dimensional metal in these cases, the fibers are expected to be metallic. The armchair tubule geometry was previously considered using a first-principles, self-consistent, all-electron Gaussian-orbital based local-density-functional calculation by Mintmire, Dunlap, and White,[3] and the tubules were shown to be metallic, with a large density of states at the Fermi level in comparison to 2D graphite.

Next we consider the armchair fiber with a screw axis as shown in Fig. 3(b). The above discussion is valid in the case of a chiral fiber if we change the boundary condition as follows:

$$\sqrt{3}N_x k_x a + N_y k_y a = 2\pi m, \quad (8)$$

in which $N_y a$ is the shift vector of the screw in the di-

TABLE I. Character table for group $D_{(2n+1)d}$ [$\phi_m = \frac{2m\pi}{2n+1}$ $(m = 1, \ldots, n)$].

$D_{(2n+1)d}$	E	$2C_{\phi_m}$	$(2n+1)C_2'$	i	$2iC_{\phi_m}$	$(2n+1)\sigma_d$
A_{1g}	+1	+1	+1	+1	+1	+1
A_{2g}	+1	+1	−1	+1	+1	−1
E_{1g}	+2	$2\cos\phi_m$	0	+2	$2\cos\phi_m$	0
E_{2g}	+2	$2\cos 2\phi_m$	0	+2	$2\cos 2\phi_m$	0
⋮	⋮	⋮	⋮	⋮	⋮	⋮
A_{1u}	+1	+1	+1	−1	−1	−1
A_{2u}	+1	+1	−1	−1	−1	+1
E_{1u}	+2	$2\cos\phi_m$	0	−2	$-2\cos\phi_m$	0
E_{2u}	+2	$2\cos 2\phi_m$	0	−2	$-2\cos 2\phi_m$	0
⋮	⋮	⋮	⋮	⋮	⋮	⋮

rection of the armchair fiber axis and m is an integer for specifying inequivalent energy bands. If we add the following rule for making a fiber that we connect the two dotted lines in Fig. 3(a) as explained in Sec. I, there is a one-to-one correspondence between a vector of (N_x, N_y) and a fiber. Especially, $(N_x, N_y) = (0, p)$ and $(q, 0)$ where p, q are integers, correspond to the zigzag and armchair fibers, respectively, and thus this expression includes both cases. When N_x and N_y are both integers or both half of odd integers, that is,

$$(N_x, N_y) = (p, q) \text{ or } (p + \tfrac{1}{2}, q + \tfrac{1}{2})$$

$$(pq \neq 0, p, q : \text{integers}), \quad (9)$$

we can make a chiral fiber. In the case of Fig. 3, N_x and N_y are $\frac{11}{2}$ and $\frac{1}{2}$, respectively. Let us adopt the unit cell and Brillouin zone for the chiral fiber which we have already used for the armchair fiber as shown in Fig. 4(a). When we put Eq. (8) into Eq. (3), eliminate k_x, and rewrite k_y as k, we get the following energy dispersion relations for chiral fibers:

$$E_m^a(k) = \pm\gamma_0 \left\{ 1 \pm 4\cos\left(\frac{m\pi}{N_x} - \frac{N_y}{N_x}\frac{ka}{2}\right)\cos\left(\frac{ka}{2}\right) + 4\cos^2\left(\frac{ka}{2}\right)\right\}^{1/2}$$

$$(-\pi < ka < \pi) \quad (m = 1, \ldots, N_x), \quad (10)$$

yielding $4N_x$ inequivalent energy bands in the generic Brillouin zone used in this work when we doubly count for the degenerate energy bands. It is stressed here that if we do not adopt any rotational boundary condition for the fibers but consider the electronic structure as a pure 1D problem, there will be many carbon atoms in the large unit cell especially for the chiral fibers. To avoid the complexity of the one-dimensional energy dispersion relations in the corresponding small Brillouin zone, we find the above treatment to be very effective. Since the atomic arrangement in the chiral fiber still gives rise to a lattice structure described by two sublattices, the calculated energy band structure consists of 1D energy dispersion relations which are obtained by slicing the 2D energy dispersion relations of graphite in the direction expressed by Eq. (8).

The condition that a fiber is metallic is that the one-dimensional band intersects the K point in the 2D graphite Brillouin zone and this is not always possible for the general chiral fiber. We found that when N_y is a half of a multiple of 3 for any N_x, the corresponding fiber can be a metal. Especially for the armchair case, where N_y=0, there is no limitation on N_x, since the metallic bands in Eq. (5) correspond to $m = N_x$.

It is noted here that the two atoms on the different sublattices remain distinct even for the chiral fiber. This implies that some chiral fibers can be metallic while others are semiconductors, depending on the geometry. It is interesting that we can have either metallic or semiconducting materials depending on the boundary conditions, without changing any hybridizations.

So far we have neglected the mixing of σ and π orbitals. For graphite, where the graphene planes are flat, there is no mixing. However, in the case of a fiber, the curvature of the fiber gives rise to some mixing of σ and π bands.[16] Here we check that this effect is small at the Fermi energy within the tight-binding approximation for σ and π bands. The secular equation we use is

$$\mathcal{H}\mathbf{c} = E\mathcal{S}\mathbf{c}, \quad (11)$$

where $\mathcal{H}$ and $\mathcal{S}$ are the Hamiltonian matrix and the overlap matrix, respectively, E and $\mathbf{c}$ are the eigenvalue and eigenvector, respectively. Usually $\mathcal{S}$ is taken as a unit matrix in the tight-binding approximation. However, when we consider the mixing of the σ and π bands, the overlap matrix $\mathcal{S}$ is necessary for determining the relative positions of the σ and π bands correctly. The matrix elements of $\mathcal{H}$ and $\mathcal{S}$ are calculated on the basis of the Bloch $2s$, $2p_x$, $2p_y$, and $2p_z$ orbitals in which only nearest-neighbor interactions are considered. As a result, we need nine tight-binding parameters as listed in Table II in which $E(2s)$ is the site energy of the $2s$ orbital relative to that of the $2p$ orbital, while $t(pp\pi)$, $t(pp\sigma)$, $t(sp)$, and $t(ss)$ are transfer integrals of π and σ bonds between $2p$ orbitals and the transfer between $2s$ and $2p$, and $2s$ and $2s$ orbitals, respectively. It is noted that the parameter γ_0 appearing in Eq. (2) and $t(pp\pi)$ are identical. The corresponding overlap integrals are denoted by $s(pp\pi)$, $s(pp\sigma)$, $s(sp)$, and $s(ss)$. These parameters are determined by fitting the energy dispersion relations of 2D graphite[17] at the K and Γ points in the graphite Brillouin zone.[18] These parameters are similar to Chadi's tight-binding parameters[19] in which he neglected the overlap integrals. In Fig. 6(a) we plot 2D energy dispersion relations of graphite using these parameters and the results reproduce very well the many significant features in 2D graphite obtained by projection of the first-principles calculations of 3D graphite.[20] We can use the same parameters in the case of the fibers, if we assume that the C-C bond length in the fiber does not change relative to that in 2D graphite. There are two possibilities for bending C-C bonds. That is, the bending occurs (1) at the atom because of the hybridization change and (2) in the overlap region of the wave functions. Since there are many possible hybridizations in carbon, it is reasonable to adopt the former case in the present calculation of the matrix elements.

Here we show only the calculated results for zigzag

TABLE II. Tight-binding parameters for 2D graphite (eV): the definition of each parameter is taken such that the overlap integrals are positive. $E(2s)$ is the energy of the $2s$ level relative to that of $2p$ (Ref. 18).

$E(2s)$	−8.868		
$t(ss)$	−6.769	$s(ss)$	0.212
$t(sp)$	−5.580	$s(sp)$	0.102
$t(pp\sigma)$	−5.037	$s(pp\sigma)$	0.146
$t(pp\pi) = \gamma_0$	−3.033	$s(pp\pi)$	0.129

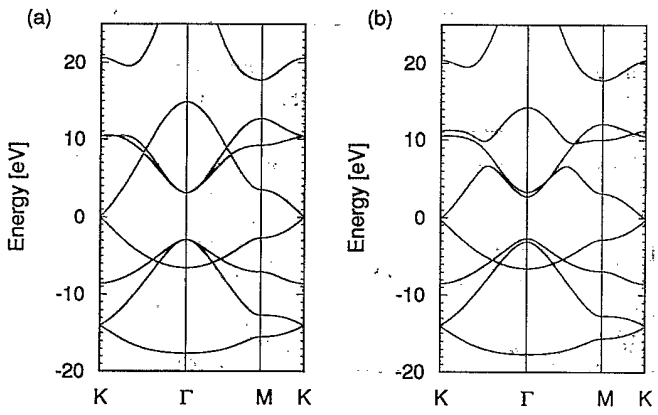

FIG. 6. 2D energy dispersion relations of (a) graphite and (b) a zigzag fiber (the σ-π mixing effect).

fibers since there is no essential difference between the zigzag, armchair, and chiral fibers. Since the energy dispersion of 2D graphite is more familiar than that of the fiber, it is easier to understand the σ-π mixing effect in the Brillouin zone of graphite. In Fig. 6(b) the 2D energy dispersion relations for a zigzag fiber are plotted. From the figure we can see that there is no significant change of the energy dispersion relations of the zigzag fibers compared with those of 2D graphite especially near the Fermi level. For the fibers we can see an enhancement of the anticrossing of the energy bands only at the crossing points of the antibonding σ and π bands. This means that the mixing of σ and π is small, since the mixing factor of $\sin(\pi/2N_x)$ with $N_x = 9$ multiplies the matrix element between the σ and π orbitals.

However, it is noted that using our calculation there is a narrow energy gap of 0.14 eV at the Fermi level for the $N_x = 9$ zigzag fiber. Thus in this case we can say that the zigzag fiber is a narrow-gap semiconductor. However, the mixing effect associated with the curvature of the cylinder produces an energy gap which decreases quickly with increasing N_x (as $\lesssim 1/N_x^2$) since the energy gap formation at the Fermi energy can be considered to be a second-order perturbation of the mixing effect. Unless the fiber diameter is smaller than $N_x = 9$, the small energy gap can be neglected at room temperature.

It is also easy to see that the second-nearest-neighbor interactions would be more sensitive to curvature than the nearest-neighbor interactions. The curvature, however, does not much affect the energy band structure even in this case, since the mixing factor is proportional to the distance d between two atoms, while the matrix elements are proportional to d^{-2} or smaller and the number of atoms is proportional to d (not d^2). Thus the mixing effect from near neighbors on the energy dispersion relations for the fibers is of the same order at most, if d is much smaller than the diameter of the fiber.

III. INSTABILITY AT THE FERMI LEVEL AND DISCUSSION

Finally we discuss the instability of the 1D energy bands. Since the one-dimensional energy bands which cross the K point of the graphite Brillouin zone have a finite density of states at the Fermi energy, these bands would be expected to be unstable against perturbations which open an energy gap at E_F and consequently lower the total energy.[13] In the case of the nanometer fibers discussed in the present work, there are some lattice distortions which couple with the electrons at the Fermi energy: (1) in-plane lattice distortions which induce the formation of Kekulé structures, and (2) out-of-plane distortions. Mintmire, Dunlap, and White have discussed case (1) and have concluded that the fibers are stable against a Peierls distortion at room temperature.[3] However, for the in-plane lattice distortion, the unit cell will be at least three times as large as that of graphite. In this case a symmetry-lowering distortion is not always possible by the boundary conditions for the general fibers.[21] On the other hand, out-of-plane vibrations do not change the size of the unit cell, but result in a different site energy for carbon atoms on A and B sites in the case of the fiber structures. Therefore we consider the out-of-phase distortions. If we do not consider the limitations imposed by the boundary conditions and the coupling constants, the discussion of the instability is similar to that of Mintmire, Dunlap, and White.[3] Further we only show the calculated result for the zigzag fibers since there is no essential difference between this result and that for all other fibers. Mintmire, Dunlap, and White[3] have given a similar discussion for the armchair tubules.

When the site energy for A and B carbon atoms is shifted by $\pm U\delta/2$ in which U is the electron-phonon coupling constant per the distortion δ, the energy dispersion of the distorted π bands of the zigzag fiber E_δ^m is expressed as

$$E_\delta^m = \pm\gamma_0 \left\{ \left(\frac{U\delta}{2\gamma_0}\right)^2 + 1 + 4\cos\left(\frac{\sqrt{3}ka}{2}\right)\cos\left(\frac{m\pi}{N_y}\right) + 4\cos^2\left(\frac{m\pi}{N_y}\right)\right\}^{1/2} . \tag{12}$$

This relation implies an energy gap of $U\delta$ at the K point. Taking account of the potential energy of the lattice as $g\delta^2/2$ per unit cell of graphite, in which g is a spring constant, we obtain the following gap equation for the zigzag fiber:

$$-\frac{g\gamma_0}{(U/2)^2} = \frac{1}{2\pi}\frac{1}{N_x}\sum_{m=1}^{N_x}\frac{1}{\sqrt{A_m + B_m}} K\left(\sqrt{\frac{2B_m}{A_m + B_m}}\right), \tag{13}$$

in which $K(x)$ is the complete ellipsoidal integral of the first kind and A_m and B_m are given by

$$A_m = \left(\frac{U\delta}{2\gamma_0}\right)^2 + 1 + 4\cos^2\left(\frac{m\pi}{N_y}\right), \qquad B_m = \left|4\cos\left(\frac{m\pi}{N_y}\right)\right|, \tag{14}$$

respectively. In Fig. 7, we plot the normalized energy gap

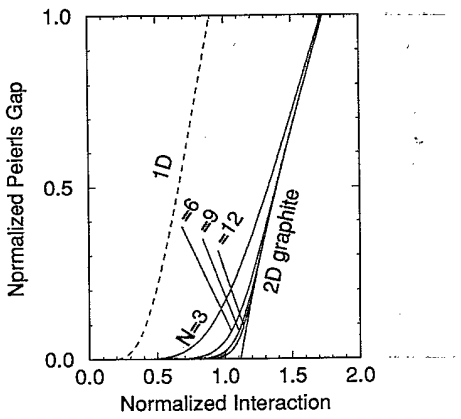

FIG. 7. Plot of normalized gap $U\delta/2\gamma_0$ vs normalized interaction $|U^2/4g\gamma_0|$ for a zigzag carbon fiber with N_y = 3, 6, 9, 12, and ∞ (2D graphite). The case of the 1D tight-binding model is also plotted for comparison.

$-(U\delta/2\gamma_0)$ as a function of the normalized intensity of the interaction of $-U^2/4g\gamma_0$ ($\gamma_0 < 0$) for special values of N_x = 3, 6, 9, 12, and $N_x = \infty$ (2D graphite). For comparison we also present data on the same plot for the 1D simple tight-binding model with the transfer energy of γ_0 for comparison and where there are two atoms at the distance of the lattice constant of a. From the figure, we see that the dependence of the energy gap of the fiber on the electron-phonon coupling constants is very close to that for the 2D case and that the energy gap is much suppressed compared with the 1D results.

If $\cos(\frac{m\pi}{N_y}) = \pm\frac{1}{2}$ in Eq. (13), there is a logarithmic singularity of the ellipsoidal function when $\delta \to 0$, which corresponds to the case where the one-dimensional bands cross the K point in the Brillouin zone without interaction. Therefore we have a nonzero value of δ which satisfies Eq. (13) for arbitrary values of U and g whenever N_y is a multiple of 3. However, the gap that forms decreases exponentially with increasing N_y as seen in the figure.[3] This means that the energy gap is negligibly small and we can neglect it, if we consider fluctuations or finite temperature effects.[22]

In the limit of $N_y \to \infty$, we can get the two-dimensional case in which a nonzero value of δ appears only when $-U^2/4g\gamma_0 > 1.117$. Since there is no experimental distortion in 2D graphite, the normalized interaction of $-U^2/4g\gamma_0$ satisfies the above condition.

IV. DISCUSSION AND CONCLUSION

It should be mentioned that in the case of a real carbon fiber it seems to be difficult to require the one-dimensional energy bands to cross just at the degenerate energy points. If we introduce anisotropy into the transfer energy, the degenerate point is still a point in the Brillouin zone, though its position is shifted from the K points. The fact that degenerate points with an energy $E = 0$ exist does not change even if we consider long-range interactions in a layer. Since the band crossings will not all coincide, it may be difficult to get metallic bands. However, if we introduce a random interaction between two graphite layers in a fiber (as would occur because of the turbostratic relation between adjacent incommensurate layers[2]) the degenerate points for the two layers will appear at somewhat different energies, which gives a small electron and hole Fermi surface near $E = 0$. In this case, it is not so difficult for a one-dimensional band to cross the Fermi surface. In this case the density of states obtained for one-dimensional energy bands at the Fermi level is much larger than that of 2D or 3D graphite.

We conclude that there are some possible carbon fibers which can be constructed from C_{60}, following the pictures in Figs. 1 and 2. Especially the screw fiber can be made easily without any distortion arising from the screw axis. The energy dispersion relations of the fiber consist of one-dimensional energy bands which arise from the slicing of 2D energy dispersion relations of a graphene sheet, and this procedure is also valid for the case of the chiral fiber. The instability generally found for 1D energy bands is greatly suppressed by the special nature of the energy dispersion of 2D graphite near the Fermi level. The fact that the band crossings just occur at the degenerate K point may apply even for realistic fibers when we consider some long-range interactions.

ACKNOWLEDGMENTS

The authors thank Dr. Katsuyoshi Kobayashi for providing us with tight-binding band parameters for 2D graphite. Two of the authors (R.S. and M.F.) have carried out this work while visiting MIT. R.S. and M.F. acknowledge financial support from the Ministry of Education, Science and Culture of Japan. We gratefully acknowledge NSF Grant No. DMR88-19896 for support for this research.

*Permanent address: University of Electro-Communications, Chofu, 182 Tokyo, Japan.
†Permanent address: Institute of Materials Science, University of Tsukuba, Tsukuba 305, Japan.

[1] M. S. Dresselhaus, G. Dresselhaus, and R. Saito, Phys. Rev. B **45**, 6234 (1992).
[2] S. Iijima, Nature (London) **354**, 56 (1991).
[3] J. W. Mintmire, B. I. Dunlap, and C. T. White, Phys. Rev. Lett. **68**, 631 (1992).
[4] P. Labastie, R. L. Whetten, H. P. Cheng, and K. Holczer (unpublished).
[5] M. S. Dresselhaus, G. Dresselhaus, K. Sugihara, I. L. Spain, and H. A. Goldberg, *Graphite Fibers and Filaments*, Springer Series in Material Science Vol. 5 (Springer-Verlag, Berlin, 1988).
[6] W. Krätschmer, L. D. Lamb, K. Fostiropoulos, and D. R.

Huffman, Nature (London) **347**, 354 (1990).
[7]R. E. Haufler, J. J. Conceicao, L. P. F. Chibante, Y. Chai, N. E. Byrne, S. Flanagan, M. M. Haley, S. C. O'Brien, C. Pan, Z. Xiao, W. E. Billups, M. A. Ciufolini, R. H. Hauge, J. L. Margrave, L. J. Wilson, R. F. Curl, and R. E. Smalley, J. Phys. Chem. **94**, 8634 (1990).
[8]G. Meijer and D. S. Bethune, Chem. Phys. Lett. **175**, 1 (1990).
[9]G. Meijer and D. S. Bethune, J. Chem. Phys. **93**, 7800 (1990).
[10]P. R. Wallace, Phys. Rev. **71**, 622 (1947).
[11]G. W. Hayden and E. J. Mele, Phys. Rev. **36**, 5010 (1987).
[12]S. Saito and A. Oshiyama, Phys. Rev. Lett. **66**, 2637 (1991).
[13]R. E. Peierls, *Quantum Theory of Solids* (Oxford University Press, London, 1955).
[14]W. P. Su, J. R. Schriefer, and A. J. Heeger, Phys. Rev. Lett. **42**, 1698 (1979); Phys. Rev. B **22**, 2009 (1980).
[15]M. S. Dresselhaus and G. Dresselhaus, Adv. Phys. **30**, 139 (1981).
[16]R. A. Jishi and M. S. Dresselhaus, Phys. Rev. B **45**, 6923 (1992).
[17]F. Bassani and G. P. Parravicini, Nuovo Cimento **50B**, 95 (1967).
[18]K. Kobayasi, (private communication).
[19]D. J. Chadi, J. Vac. Sci. Technol. A **2**, 948 (1984).
[20]See, for example, C. Fretigny, R. Saito, and H. Kamimura, J. Phys. Soc. Jpn. **58**, 2098 (1989).
[21]K. Harigaya, Phys. Rev. B **45**, 12071 (1992).
[22]H. Zheng, D. Feinberg, and M. Avignon, Phys. Rev. **39**, 9405 (1989).